Programmable Microwave and Optical Pulse Generation Based on Coupled Optoelectronic Oscillator

Li Yang, Shifeng Liu, Changlong Du, Mingzhen Liu, and Shilong Pan, *Fellow, IEEE*

***Abstract*—We propose and experimentally demonstrate a method for generating programmable microwave and optical pulses using a coupled optoelectronic oscillator (COEO). An external low-frequency electrical signal is injected into both the optical fiber loop and optoelectronic loop of the COEO through a shared intensity modulator. When the period of the external signal matches the round-trip time of the optical fiber loop, it modulates the gain in both loops. Once the gain exceeds unity, microwave and optical pulses are generated in the respective loops. The durations and positions of these pulses within each period directly correspond to those of the external signal. Therefore, by manipulating the external signal, the durations and positions of the microwave and optical pulses can be flexibly controlled. In a proof-of-concept experiment, the proposed scheme initially generates a 9.985-GHz sinusoidal microwave signal along with an 11.47-ps optical pulse. The repetition rate of the optical pulses matches the frequency of the microwave signal. Subsequently, by controlling the external signals, microwave and optical pulse signals with duty cycles of 30%, 50%, and 70% are generated within a single period. Additionally, when external signals with double-pulse waveforms and programmable durations and positions are applied, the corresponding microwave and optical pulses are generated by the proposed scheme. The experimental results confirm that by programming the external signals, fully programmable microwave and optical pulses can be successfully generated.**

***Index Terms*—Coupled optoelectronic oscillator, gain control, programmable microwave and optical pulse generation.**

I. Introduction

MICROWAVE pulses are widely used in modern radar systems, communication systems, and electronic warfare [1], [2], [3]. Programmable microwave pulses enable flexible control over pulse position and duration, thereby mitigating multipath effects in radar systems [4], enhancing anti-jamming performance in communication systems [5], and deceiving enemy radar in electronic warfare scenarios [6], [7]. Similarly, optical pulses are widely used in metrology, micromachining, and optical communication systems [8], [9]. Programmable optical pulses enable adaptability to diverse measurement requirements in metrology systems [10], prevent excessive heat accumulation in micromachining [11], and provide precise control over pulse parameters in optical communication systems, thereby reducing noise, minimizing interference, and lowering bit error rates [12]. The simultaneous generation of microwave and optical pulses eliminates the need for separate signal sources, simplifies system architecture, and enables the integration of optical communication and radar sensing.

Microwave pulses generated by optoelectronic oscillators (OEOs) have attracted increasing attention due to their low phase noise and high spectral purity. This type of pulse generation is typically realized by periodically modulating the loop gain of the OEO based on the principle of active mode-locking. In actively mode-locked OEOs, an external signal with a repetition frequency equal to an integer multiple of the loop's free spectral range (FSR) is injected through an electro-optic modulator or an auxiliary optical or electrical modulator. This signal modulates the loop gain, thereby enabling the generation of microwave pulses [13], [14], [15], [16], [17], [18], [19], [20], [21], [22], [23], [24]. The repetition frequency of the generated microwave pulses is tunable and corresponds to an integer multiple of the FSR [13], [14], [15], [16], [17], [18], [19], [20]. In addition to adjustable repetition frequency, studies have demonstrated that the shape, duration, and position of generated microwave pulses can be programmed by tailoring the external signal [21], [22], [23], [24]. In [25], a Fourier domain mode-locked optoelectronic oscillator (FDML-OEO) was employed to generate microwave pulses with varying duty cycles. However, these methods are limited to generating microwave pulses and cannot simultaneously produce corresponding optical pulses.

Common approaches for generating optical pulses include passive and active mode locking, as well as exploiting Kerr or electro-optical nonlinearities in optical fibers [26], [27], [28]. However, the optical pulses generated by these methods typically exhibit fixed repetition intervals. Optical pulses with variable intervals and counts can be generated using acousto-optic [29] or electro-optic [30] modulator-based pulse pickers.

Received 19 May 2025; revised 14 July 2025; accepted 1 August 2025. Date of publication 6 August 2025; date of current version 2 October 2025. This work was supported in part by National Key R&D Program of China under Grant 2022YFB2802704, in part by the Jiangsu Funding Program for Excellent Postdoctoral Talent under Grant 2022ZB237, in part by the National Natural Science Foundation of China under Grant 62271249, and in part by the National Natural Science Foundation of China under Grant 62071226. *(Corresponding author: Shifeng Liu.)*

The authors are with the National Key Laboratory of Microwave Photonics, Nanjing University of Aeronautics and Astronautics, Nanjing 210016, China (e-mail: liyang_photonic@nuaa.edu.cn; sfliu_nuaa@nuaa.edu.cn; changlongdu@nuaa.edu.cn; liumingzhen@nuaa.edu.cn; pans@nuaa.edu.cn).

Color versions of one or more figures in this article are available at https://doi.org/10.1109/JLT.2025.3596454.

Digital Object Identifier 10.1109/JLT.2025.3596454

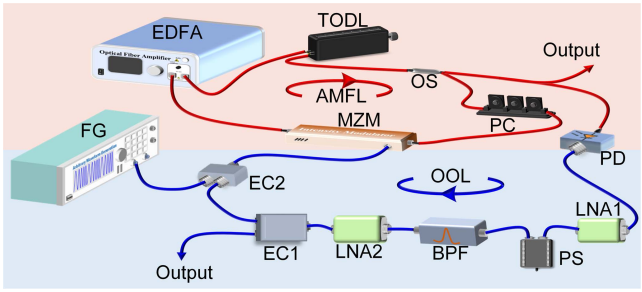

Fig. 1. Schematic of the proposed scheme for programmable microwave and optical pulses generation. EDFA: Erbium-doped fiber amplifier; TODL: Tunable optical delay line; OS: Optical splitter; PC: Polarization controller; MZM: Mach-Zehnder modulator; PD: Photodetector; LNA: Low-noise amplifier; PS: Phase shifter; BPF: Band-pass filter; EC: Electrical coupler; FG: Function generator.

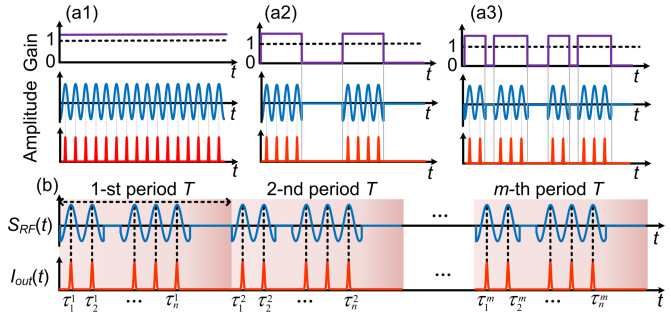

Fig. 2. (a) Schematic diagram of COEO under different external signals. (b) Schematic diagram of AMFL generating programmable optical pulses in COEO.

Programmable optical waveforms have also been achieved by adjusting the gain of a semiconductor optical amplifier within an optical cavity [31]. However, these methods have difficulty generating short-interval optical pulses. Adjustable-position optical pulses have been demonstrated in [32] and [33] using the Talbot effect in a frequency-shifted fiber loop and active mode-locking, respectively. However, both methods require injecting high-frequency electrical signals into the optical cavity to generate optical pulses with narrow intervals.

In this paper, we propose and experimentally demonstrate a scheme for generating programmable microwave and optical pulses within one period using a coupled optoelectronic oscillator (COEO). To date, no existing approach has been capable of simultaneously generating programmable microwave and optical pulses. In this work, we employ a COEO with gain modulation to simultaneously generate programmable microwave and optical pulses, providing precise control over their durations and positions within each period. In the proposed approach, a low-frequency external electrical signal is utilized to control the gain of the optoelectronic oscillation loop (OOL) and the active mode-locked fiber loop (AMFL) within the COEO. When the repetition period of the external signal matches the round-trip time of AMFL and the loop gain exceeds unity, microwave and optical pulses are generated with durations and positions defined by the external signal. By manipulating the external signal, the proposed scheme enables the generation of programmable microwave and optical pulses.

II. Principle

Fig. 1 illustrates the schematic of the proposed system for generating programmable microwave and optical pulses using a COEO. The COEO primarily comprises an OOL and an AMFL, interconnected via a Mach-Zehnder modulator (MZM) and a photodetector (PD). In the AMFL, an erbium-doped fiber amplifier (EDFA) serves as the light source, providing spontaneous emission as the initial optical signal. The optical signal then passes through a tunable optical delay line (TODL) and is split into two paths by an optical splitter (OS). One part is directed to the PD for conversion into an electrical signal, while the other passes through a polarization controller (PC) to adjust its polarization state before entering the MZM. The optical signal exiting the MZM is fed back into the EDFA, completing the fiber loop. The electrical signal from the PD is first amplified by a low-noise amplifier (LNA1), and then passed through a phase shifter (PS) for phase adjustment. The phase-shifted signal is filtered by a wideband bandpass filter (BPF) and amplified by the LNA2. The amplified electrical signal is divided into two paths: one serves as the output, while the other is combined with the low-frequency external signal from a function generator (FG) using an electrical coupler (EC2) and fed back into the MZM, completing the optoelectronic loop.

When FG is turned off, the system operates as a conventional free-running COEO [34]. The circulating optical modes in the fiber loop are converted into electrical signals by the PD. After passing through the BPF, only modes within its bandwidth are preserved and amplified in the optoelectronic loop. These filtered modes are re-injected into the fiber loop by MZM. The TODL and PS are adjusted to align their phases with the existing modes in both loops. The OOL generates a single-frequency signal at $f_0 = N*\mathrm{FSR}$, where N is a positive integer and f_0 corresponds to the center frequency of the BPF. The fiber loop functions as an AMFL, generating optical pulses with a repetition rate matching f_0. When FG is turned on, the behaviors of both the OOL and AMFL deviate from those of a conventional COEO. Specifically, when an external signal from the FG, with a period matching the loop's round-trip time, is injected into the AMFL by MZM, the phase of the mode is locked to the external signal. These optical modes are converted into electrical signals via the PD and subsequently enter the OOL. The mode located near f_0 within the BPF passband is also locked by the external signal, and the spacing between the locked modes is equal to the frequency of the injected signal. Consequently, the OOL generates a microwave pulse with a period matching that of the external signal. Simultaneously, as described in [33], the AMFL generates corresponding optical pulses synchronized with the microwave pulse.

Fig. 2(a) illustrates schematic diagrams of programmable microwave and optical pulses generation by the COEO under three different external signal conditions. When no external signal is applied, the gain within the loops and the signals generated by the system are shown in Fig. 2(a1). The gain remains constant, as indicated by the purple line. When this gain exceeds the oscillation threshold (black dashed line), the OOL and AMFL generate

continuous microwave and optical pulses, represented by the blue and red solid lines, respectively. The repetition frequency of the optical pulses matches that of the microwave signal, both determined by the center frequency of the BPF. Fig. 2(a2) shows the case where an external signal with a fixed duration is applied. This signal is injected into both the AMFL and OOL via the MZM, with a period matching the round-trip time of the AMFL. Due to the loss modulation effect of the MZM, the gain profile follows the shape of the external signal. Microwave and optical pulses are generated at time intervals where the net gain (purple solid line) exceeds the oscillation threshold (black dashed line), indicating that both types of pulses have the same duration as the external signal. Fig. 2(a3) presents the case where the external signal has a double-pulse shape, featuring two high-level segments of different durations. This signal, with a period matching that of the AMFL, is similarly injected into both loops. The resulting microwave and optical pulses, represented by the red and blue solid lines, respectively, occur at durations and positions corresponding to the external signal within each period. These results demonstrate that by adjusting the duration and positions of the external signal, programmable generation of microwave and optical pulse signals can be flexibly achieved.

Since the COEO consists of both the OOL and AMFL, the output signal in the OOL can be expressed as follows, based on reference [35]:

$$V_{out}(t) = V_{ph}\left\{1-\sin\left[\pi V_{in}(t)/V_\pi + \pi V_{EDS}(t)/V_\pi + \pi V_B/V_\pi\right]\right\} \quad (1)$$

where $V_{\mathrm{out}}(t)$ represents the output signal from the RF amplifier in the oscillation loop, and $V_{\mathrm{in}}(t)$ and $V_{\mathrm{EDS}}(t)$ represent the input signal and the external signal applied to the RF port of the MZM, respectively. Equation (1) shows that the OOL output signal is determined by the input signal, the external signal, and the bias voltage of the MZM.

The expression for calculating V_{ph} in (1) is given by:

$$V_{ph} = \Re R_{\mathrm{Load}} G_A(\alpha P_0/2) \quad (2)$$

where R_{Load} and $\Re$ are the load impedance and responsivity of the PD, respectively; G_A denotes the amplifier gain, α represents the optical path loss, P_0 is the optical power input to the PD; and V_π and V_{B} denote the half-wave voltage and the direct-current bias voltage of the MZM, respectively.

By combining (1) and (2), the open-loop gain of the OOL can be expressed as:

$$G_S = \left.\frac{dV_{out}}{dV_{in}}\right|_{V_{in}=0} = -\frac{\pi V_{ph}}{V_\pi}\cos\left(\frac{\pi V_{EDS}(t)}{V_\pi}+\frac{\pi V_B}{V_\pi}\right) \quad (3)$$

The MZM in the COEO operates at its linear transmission point, with the bias voltage fixed at $V_B = V_\pi/2$. According to (3), the open-loop gain of the OOL is determined by $V_{EDS}(t)$ [23]. When no external signal is injected into the COEO, i.e., $V_{EDS}(t) = 0$, the open-loop gain remains constant. Under this condition, the COEO functions as a conventional oscillator, generating a continuous microwave signal and optical pulses, as shown in Fig. 2(a1). When an external signal is applied, the loop gain is modulated accordingly. Once the loop gain exceeds unity, the OOL generates a microwave pulse signal whose period and duration match those of the external signal, as shown in Fig. 2(a2). By adjusting the external signal, the duration and position of the generated microwave pulse can be flexibly programmed, as illustrated by the blue solid line in Fig. 2(a3).

In an AMFL, when an arbitrary waveform is applied to the intensity modulator, the waveform precisely determines the point of minimum cavity loss within each round-trip time [33]. In the proposed scheme, a microwave signal with programmable duration and position is generated by modulating the loop gain in the OOL, as previously described. The generated microwave signal is subsequently used as the electrical driving signal for the AMFL. The period of the microwave signal matches the round-trip time of the fiber loop, and optical pulses are generated at the point of minimum loss within each round trip, as indicated by the red curves in Fig. 2(a2) and (a3).

To clarify the mechanism of programmable optical pulse generation in the AMFL of the COEO, an analytical diagram is presented in Fig. 2(b). In Fig. 2(b), the blue solid line represents the electrical signal injected into the cavity via the MZM, corresponding to the microwave signal from the OOL, while the red solid line represents the generated optical pulse. According to [33], the envelope of the optical pulse is expressed as:

$$I_p(t) \propto E_0^2 \frac{\sin^2[(2M+1)(\Delta\omega t+\theta)/2]}{\sin^2[(\Delta\omega t+\theta)/2]} \quad (4)$$

where E_0 is the amplitude of the longitudinal mode in the fiber loop, $2M+1$ denotes the total number of longitudinal modes in the optical fiber loop contributing to the optical pulse, $\Delta\omega = 2\pi/T_{\mathrm{r}}$ is the angular frequency spacing between adjacent modes in the AMFL, $T_{\mathrm{r}} = 1/\mathrm{FSR}$ is the round-trip time of the AMFL, and θ is the fixed phase difference between adjacent modes.

According to (4), $I_p(t)$ reaches its peak when $\Delta\omega t+\theta = 2k\pi$ (with $k = 0, 1, 2,..., m$, and m is a positive integer). Hence, $I_p(t)$ represents the envelope of the optical pulse at position ${\tau_1}^1$, ${\tau_1}^2$, …, ${\tau_1}^m$. As shown in Fig. 2(b), the optical pulse $I_{out}(t)$ generated by the AMFL consists of m periods, each with a duration T, where $T = T_{\mathrm{r}}$. Each period T contains n pulses, with their positions denoted by ${\tau_1}^i$, ${\tau_2}^i$, …, ${\tau_n}^i$, where i represents the i-th period ($i = 1, 2, \ldots, m$). The number of pulses n and their positions within each period are determined by the microwave pulse from the OOL injected into the MZM. Therefore, the optical pulse $I_{out}(t)$ can be considered as a chain of n pulses, each with an interval of T, starting at ${\tau_1}^1$, ${\tau_2}^1$, …, ${\tau_n}^1$. Thus, the output optical pulse $I_{out}(t)$ can be expressed as:

$$I_{out}(t) = \sum_{p=1}^{n} I_p(t) = \sum_{p=1}^{n} \frac{\sin^2\{(2M+1)[\Delta\omega(t-\tau_p^1)+\theta]/2\}}{\sin^2[\Delta\omega(t-\tau_p^1)/2+\theta/2]} \quad (5)$$

According to (5), a programmable microwave pulse injected into the AMFL generates a corresponding optical pulse. Therefore, when a low-frequency external electrical signal is injected into the COEO, the OOL produces a programmable microwave

pulse, thereby enabling the generation of programmable optical pulses in the AMFL.

III. Experimental and Result

A proof-of-concept experiment for programmable microwave and optical pulse generation based on COEO was conducted, with the experimental setup depicted in Fig. 1. Key information about the devices used in the experiment is presented. The in-loop EDFA (AEDFAPAP35-B-FA, Amonics) has an adjustable pump current and provides a maximum gain of 35 dB. The TODL offers a delay range of 0 to 700 ps. The OS has a power splitting ratio of 10:90. The MZM (CETC GC15MZPE8715) has a bandwidth of 20 GHz, an insertion loss of 2.5 dB, and a half-wave voltage of 4.99 V. It operates at its linear bias point. The total optical path length is approximately 34.77 m, corresponding to a FSR of 5.87 MHz and a round-trip time of 170.35 ns.

The PD has a bandwidth of 18 GHz and a responsivity of 0.80 A/W. Both low-noise amplifiers (LNA1 and LNA2), operating from 2 to 18 GHz, provide a gain of 20 dB. The PS operates over a frequency range from DC to 18 GHz. The BPF (TLDBF-10G-E) has a center frequency of 10 GHz, a bandwidth of 100 MHz, and an insertion loss of 1.08 dB. The EC1, operating over a frequency range from 2 to 18 GHz, has a power splitting ratio of 1:1. The EC2 operates from DC to 26 GHz with a 1:1 splitting ratio. The FG (RIGOL DG4202) has a 200-MHz bandwidth, a 500-MSa/s sampling rate, and 2 channels. The period of the external electrical signal from the FG is 170.35 ns, matching the round-trip time of the AMFL. The output signal from the AMFL is directed into an optical sampling oscilloscope to obtain the optical pulse. The electrical signals from the EC1 are captured using a 50-GS/s real-time oscilloscope (DSA72004B, Tektronix) for time-domain waveform measurements, while the frequency spectra are acquired using a spectrum analyzer (PXA N9030B, Keysight ESA). The phase noise of the generated microwave signal is measured using a phase noise analyzer (FSWP26, R&S), which also supports spectrum analysis.

A. Continuous Signal Generation

Continuous optical pulse and microwave signal generation by the COEO was demonstrated without external signal injection. In the experiment, the EDFA pump current was set to 164 mA, and the FG was turned off. Compared with the conventional COEO, the proposed scheme incorporates a broadband BPF in the OOL. The passband of the BPF is significantly wider than the mode spacing of the AMFL. Within the BPF passband, multiple modes from the AMFL are amplified and oscillate in the OOL. By tuning the PS and TODL in the loops, one mode in both the OOL and AMFL can be aligned to achieve maximum gain, while other modes are suppressed. As a result, the OOL and AMFL generate a microwave signal and an optical pulse, respectively. The experimental results are shown in Fig. 3.

Fig. 3(a) and (b) show the spectrum and phase noise curve of the microwave signal, respectively. With a 1-GHz frequency span and a 1-kHz resolution bandwidth (RBW), the main mode

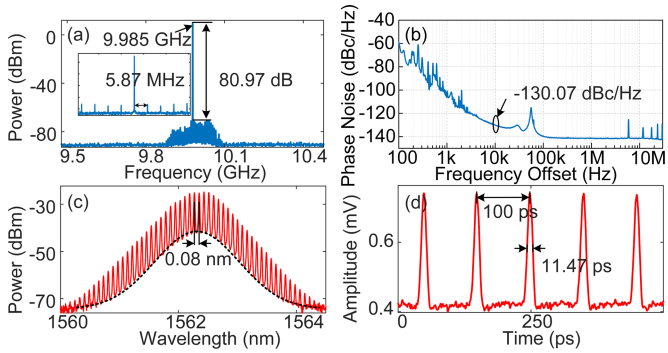

Fig. 3. (a) Electrical spectrum, and (b) single-sideband phase noise curves of the generated microwave signal in the OOL. (c) Optical spectrum and (d) optical pulses of the output signal from the AMFL.

is located at 9.985 GHz, and the side-mode suppression ratio (SMSR) reaches 80.97 dB, as shown in Fig. 3(a). The inset in Fig. 3(a) displays the electrical spectrum within a 50-MHz frequency span. The spacing between side modes is 5.87 MHz, corresponding to the FSR of the AMFL. The frequency of the microwave signal is nearly equal to the center frequency of the BPF. The side modes observed in Fig. 3(a) are mainly due to the fact that the BPF bandwidth (100 MHz) is larger than the mode spacing (5.87 MHz). The phase noise of the microwave signal is presented in Fig. 3(b), reaching −130.07 dBc/Hz at a 10-kHz offset. Fig. 3(c) and (d) illustrate the optical spectrum and the corresponding optical pulse in the AMFL, respectively. As shown in Fig. 3(c), the optical spectrum exhibits a series of comb lines spaced at 0.08 nm, superimposed on a Gaussian-shaped envelope indicated by black dotted lines. The optical pulse shown in Fig. 3(d) has a period of 100 ps and a full width at half maximum (FWHM) of 11.47 ps. The pulse period matches the 0.08-nm comb spacing, both approximately corresponding to the main mode frequency of the OOL. As demonstrated in Fig. 3, the proposed structure enables the generation of continuous microwave signals with high spectral purity, along with optical pulses featuring narrow temporal spacing and short pulse width.

B. Different Duration Signal Generation

In this section, microwave and optical pulses with varying durations are generated using the proposed scheme. The FG provides two channels: one generates a square wave signal injected into the proposed scheme, and the other outputs an electrical signal with the same frequency to serve as a trigger for an optical sampling oscilloscope. The square waves with varying duty cycles, serving as external electrical signals of different durations, are combined with the microwave signal in the OOL and injected into both the AMFL and OOL. The period of the square wave, with duty cycles of 30%, 50%, and 70%, is set equal to the round-trip time of the AMFL. The pump current of the EDFA is adjusted to ensure that the gain profile, shaped like the square wave, exceeds the oscillation threshold during its high level, thereby generating microwave and optical pulses. In the experiment, the pump current of the EDFA was 154 mA. The voltage of the square wave signals from FG was 4.05 V. The PS

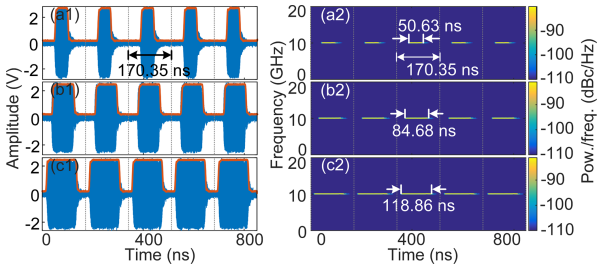

Fig. 4. (a1)–(c1) The temporal waveform of the generated microwave signal under 30%, 50% and 70% square wave injected. (a2)–(c2) Time-frequency diagram corresponding to different duty cycles.

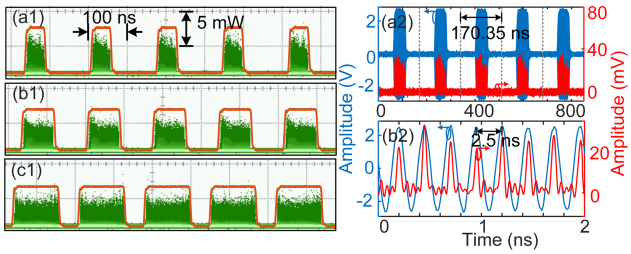

Fig. 5. (a1)–(c1) Optical pulses with duty cycles of 30%, 50%, and 70%, respectively. (a2) Temporal waveform of the microwave and optical pulses. (b2) Microwave carrier and corresponding optical pulse train within a 2-ns time window.

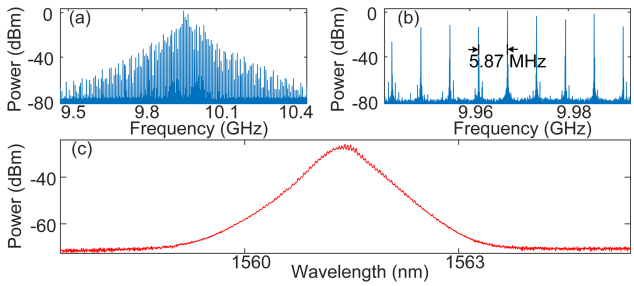

Fig. 6. The spectrum corresponding to the signal with a duty cycle of 30%. (a) and (b) The electrical spectrum of microwave pulses in the frequency range of 1 GHz and 50 MHz. (c) The optical spectrum of optical pulses.

in the optoelectronic loop was tuned to ensure microwave and optical pulses generation. Figs. 4 to 6 display the spectra and waveforms of the generated microwave and optical pulses under square wave injections with duty cycles of 30%, 50%, and 70%.

Fig. 4 shows the waveforms and time-frequency diagrams of the generated microwave pulses using the proposed scheme. In Fig. 4(a1)–(c1), the orange and blue lines represent the square waves generated by the FG and the corresponding microwave pulses, respectively. By applying the short-time Fourier transform to the microwave pulses in Fig. 4(a1)–(c1), the corresponding time-frequency diagrams are obtained and shown in Fig. 4(a2)–(c2). The generated microwave pulses have a period of 170.35 ns, consistent with that of the square waves. As shown in Fig. 4(a2)–(c2), the durations of the microwave pulses are 50.63 ns, 84.68 ns, and 117.86 ns for duty cycles of 30%, 50%, and 70%, respectively. These measured durations deviate slightly from the theoretical values of 51.10 ns, 85.18 ns, and 119.25 ns, mainly due to the bias point offset of the modulator, which introduces distortion in the gain curve.

An optical sampling oscilloscope operating in eye diagram mode is used to capture the optical pulses generated by the proposed scheme. The captured optical pulses are shown in Fig. 5(a1)–(c1). In Fig. 5(a1)–(c1), the green waveform represents the optical pulses, while the orange solid line indicates the square waves generated by the FG. As shown in Fig. 5(a1)–(c1), the period and duration of the generated optical pulses are consistent with those of the square waves injected into the COEO. Adjusting the time window of the sampling oscilloscope results in a noise-like signal. This is primarily due to the timing jitter of the low-frequency trigger signal and the sampling process of the optical sampling oscilloscope, which limit the time jitter of the acquired optical pulse waveform. Microwave pulses with a 4-GHz carrier and optical pulses with a 2.5-ns interval were generated by replacing the BPF in the OOL with one centered at 4 GHz. The experimental results, recorded using the real-time oscilloscope, are shown in Fig. 5(a2) and (b2), where the blue and red curves represent the microwave and optical pulses, respectively. As shown in Fig. 5(a2), both signals exhibit a 30% duty cycle. In the 2-ns time window of Fig. 5(b2), the microwave carrier is well aligned with the optical pulse train, consistent with theoretical expectations.

The spectrum of the 50.63-ns microwave pulse generated by the proposed scheme is shown in Fig. 6. Fig. 6(a) and (b) show the electrical spectra of the microwave pulses. Fig. 6(a) shows the spectrum over a 1-GHz frequency span. The mode spacing in the electrical spectrum corresponds to the 5.87-MHz FSR of the AMFL, as shown in Fig. 6(b). The primary reason for the spectral differences between Figs. 6 and 3 is the injection of a square wave via the MZM. The signal enables active mode-locking, which phase-locks the modes in the loop with a mode spacing of 5.87 MHz. As shown in Fig. 6(a) and (b), compared to Fig. 3(a), multiple phase-locked modes are centered within the BPF but extend beyond its 3-dB bandwidth due to the existence of the shape factor. In the optical domain, the closely spaced modes in the optical loop with a 5.87-MHz interval cannot be clearly resolved because of the limited resolution of the optical spectrum analyzer. Therefore, unlike in Fig. 3(c), the spectrum shown in Fig. 6(c) does not exhibit combs. In summary, by injecting square waves with varying duty cycles, the proposed scheme successfully generates microwave and optical pulses with controllable durations.

C. *Programmable Signal Generation*

This section presents experimental demonstrations of the proposed system's ability to generate microwave and optical pulses with programmable durations and positions. First, the generation of microwave and optical pulses with fixed durations and variable positions was verified. Subsequently, the system's ability to produce signals with both controllable durations and positions was verified. To clearly demonstrate position controllability, dual-pulse waveforms are used as the external signal injected into the proposed system.

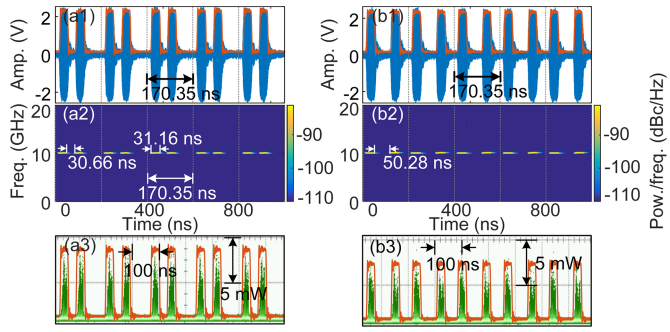

Fig. 7. The generated microwave signal and optical pulse under the fixed duration and different intervals. (a1) and (b1) The temporal waveform of the microwave signal. (a2) and (b2) The time-frequency diagram of the microwave signal. (a3) and (b3) The generated optical pulses.

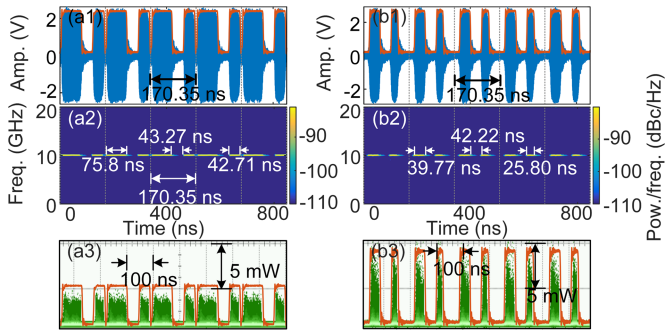

Fig. 8. The generated microwave signal and optical pulse under the different durations and intervals. (a1) And (b1) The temporal waveform of the microwave signal. (a2) And (b2) The time-frequency diagram of the microwave signal. (a3) And (b3) The generated optical pulses.

External signals consisting of dual pulses with fixed durations of 31.16 ns and varying intervals of 30.66 ns and 50.28 ns are generated by the FG and injected into the MZM. The period of the external signals is 170.35 ns, matching the round-trip time of the AMFL. The pump current of the EDFA was 124 mA, and the microwave and optical pulses with fixed durations and variable intervals were generated by the proposed scheme. The corresponding experimental results are shown in Fig. 7. In Fig. 7(a1) and (b1), the orange and blue lines represent the external signals from the FG and the microwave pulses generated by the proposed scheme, respectively. The durations and intervals of the generated microwave pulses match those of the external signals. Fig. 7(a2) and (b2) show the time-frequency diagrams corresponding to the microwave pulse signals in Fig. 7(a1) and (b1). The microwave pulses have a duration of 31.16 ns, with pulse intervals of 30.66 ns and 50.28 ns, respectively. The optical pulses generated by the proposed scheme are shown in Fig. 7(a3) and (b3), where the green waveforms represent the optical pulses and the orange solid lines denote the external signals. The intervals of the optical pulses are consistent with those of the external signals, confirming that the positions of the optical pulses are controlled by the injected waveform.

To verify the proposed scheme's capability to generate signals with controllable positions and durations, external signals with programmable features are generated by the FG and injected into the system. In Fig. 8(a1) and (b1), the microwave pulses (blue lines) closely match the external electrical signals (orange lines). Fig. 8(a2) and (b2) display the time-frequency diagrams corresponding to the microwave pulses in Fig. 8(a1) and (b1). As shown in Fig. 8(a2), microwave pulses with durations of 75.8 ns and 42.71 ns are generated, separated by 43.27 ns. Similarly, Fig. 8(b2) shows microwave pulses with durations of 39.77 ns and 25.80 ns, separated by 42.22 ns. A comparison of Fig. 8(a) and (b) reveal that the generated microwave pulses have different durations and positions that precisely match the external signals. The optical pulses generated by the proposed scheme are shown in Fig. 8(a3) and (b3), where the green waveforms represent the optical pulses and the orange solid lines denote the external signals. The intervals and durations of the optical pulses are consistent with those of the external signals.

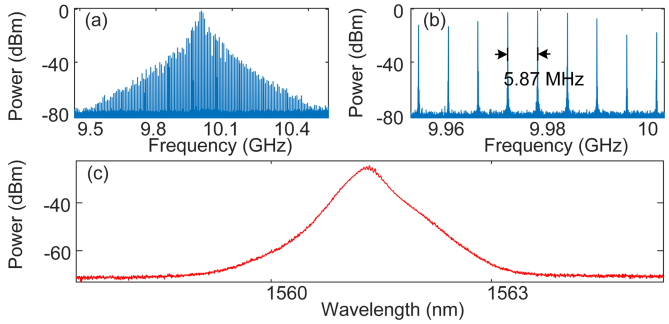

Fig. 9. (a) And (b) The electrical spectrum corresponding to the microwave signal of Fig. 7(a1). (c) The optical spectrum corresponding to the optical pulse of Fig. 7(a3).

Based on the experimental results shown in Figs. 7 and 8, the durations and positions of the generated microwave and optical pulses are clearly determined by external signals.

Fig. 9 presents the spectra of the programmable microwave and optical pulses corresponding to Fig. 7. Fig. 9(a) and (b) show the electrical spectrum of the programmable microwave pulse from Fig. 7(a1), with a RBW of 1 kHz and frequency spans of 1 GHz and 50 MHz, respectively. The oscillation modes in the OOL exhibit a spacing of 5.87 MHz, as shown in Fig. 9(b). Observed on both sides of the oscillation mode in Fig. 9(b) mainly originates from the programmable external signals generated by the FG. Fig. 9(c) shows the optical spectrum of the programmable optical pulse corresponding to Fig. 7(a3). In summary, by injecting programmable dual-pulse waveforms with varying durations and positions within one period, the proposed scheme enables the generation of microwave and optical pulses with controllable durations and positions.

IV. Conclusion

In summary, a novel approach for generating programmable microwave and optical pulses based on a COEO is proposed and experimentally demonstrated. Theoretical analysis reveals that the gain profile replicates the shape of the external signal and that the optical pulses generated are directly correlated with the microwave signals injected into the MZM. By tailoring the external signals, microwave signals with controllable durations

and positions are generated in the OOL, while corresponding optical pulses are simultaneously produced in the AMFL. Experimental results show that without external signal injection, the proposed scheme achieves the SMSR of 80.97 dB for the generated continuous microwave signal, a phase noise of −130.07 dBc/Hz at 10-kHz offset for a 9.985-GHz sinusoidal signal, and an optical pulse FWHM of 11.47 ps. When square waves with varying duty cycles are injected as external signals through the MZM, microwave and optical pulses with different durations within one period are successfully generated. Similarly, applying external signals with fixed durations and varying positions results in microwave and optical pulses with matching durations and positions. Finally, by programming the duration and position of the external signal within one period, fully programmable microwave and optical pulses are successfully generated. This scheme offers a flexible and integrated solution for advanced radar, communication, and signal processing applications.

REFERENCES

[1] M. Skolnik, *Radar Handbook*, 3rd ed. Columbus, OH, USA: McGraw-Hill, 2008.

[2] S. Pan and Y. Zhang, "Microwave photonic radars," *J. Lightw. Technol.*, vol. 38, no. 19, pp. 5450–5484, Oct. 2020.

[3] S. Ayhan, S. Scherr, A. Bhutani, B. Fischbach, M. Pauli, and T. Zwick, "Impact of frequency ramp nonlinearity, phase noise, and SNR on FMCW radar accuracy," *IEEE Trans. Microw. Theory Techn.*, vol. 64, no. 10, pp. 3290–3301, Aug. 2016.

[4] H. Zhang, L. Chen, and G. Wei, "Waveform design of spectrum sharing radar in a multi-path scenario," in *Proc. IEEE 98th Veh. Technol. Conf.*, 2023, pp. 1–6.

[5] J. Luo, S.-W. Wong, and X. Zhang, "An adaptive beamforming anti-interference system based on software-defined radio," in *Proc. Cross Strait Radio Sci. Wireless Technol. Conf.*, 2024, pp. 1–3.

[6] F. A. Butt and M. Jalil, "An overview of electronic warfare in radar systems," in *Proc. Int. Conf. Technolog. Adv. Elect., Electron. Comput. Eng.*, 2013, pp. 213–217.

[7] D. Zhu and S. Pan, "Broadband cognitive radio enabled by photonics," *J. Lightw. Technol.*, vol. 38, no. 12, pp. 3076–3088, Jun. 2020.

[8] C. Dorrer, "Spatiotemporal metrology of broadband optical pulses," *IEEE J. Sel. Top. Quantum Electron.*, vol. 25, no. 4, Jul./Aug. 2019, Art. no. 3100216.

[9] O. Wada, "Femtosecond all-optical devices for ultrafast communication and signal processing," *New J. Phys.*, vol. 6, no. 1, p. 183–216, Jan. 2004.

[10] E. D. Caldwell, L. C. Sinclair, N. R. Newbury, and J.-D. Deschenes, "The time-programmable frequency comb and its use in quantum-limited ranging," *Nature*, vol. 610, no. 7933, pp. 667–673, Oct. 2022.

[11] G. Mincuzzi et al., "Pulse to pulse control for highly precise and efficient micromachining with femtosecond lasers," *Opt. Exp.*, vol. 28, no. 12, pp. 17209–17218, May 2020.

[12] X. Xu et al., "A nonlinearity-tolerant frequency domain root M-shaped pulse for coherent optical communication systems," *Opt. Exp.*, vol. 21, no. 26, pp. 31966–31982, Dec. 2013.

[13] C. Lin, Y. Wang, A. Wang, J. Zhang, and X. Peng, "Active mode lock optoelectronic oscillator based on the simulated Brillouin scattering effect," *Appl. Opt.*, vol. 61, no. 24, pp. 7071–7077, Aug. 2022.

[14] M. Liu, S. Liu, L. Yang, C. Du, H. Liu, and S. Pan, "Improving the quality of arbitrary periodic waveform via injection-locking of an optoelectronic oscillator," *IEEE Trans. Microw. Theory Techn.*, vol. 72, no. 11, pp. 6678–6685, Nov. 2024.

[15] Y. Zhang et al., "Actively mode-locked modulator-free optoelectronic oscillator for multi-functional microwave pulse generation," *J. Lightw. Technol.*, vol. 42, no. 19, pp. 6760–6766, Oct. 2024.

[16] J. Wo, J. Zhang, and Y. Wang, "Actively mode-locked optoelectronic oscillator for microwave pulse generation," *Opt. Laser Technol.*, vol. 146, Feb. 2022, Art. no. 107563.

[17] B. Wang, Y. Liu, Y. Jiang, R. Yan, and W. Zhang, "Frequency-tunable microwave pulse generation using a dual-drive active mode-locked optoelectronic oscillator," *J. Lightw. Technol.*, vol. 42, no. 23, pp. 8221–8228, Dec. 2024.

[18] Z. Zeng et al., "Microwave pulse generation via employing an electric signal modulator to achieve time-domain mode locking in an optoelectronic oscillator," *Opt. Lett.*, vol. 46, no. 9, pp. 2107–2110, May 2021.

[19] B. Yang, J. Yu, H. Chi, S. Yang, Y. Zhai, and J. Ou, "Polarization multiplexed active mode-locking optoelectronic oscillator for frequency tunable dual-band microwave pulse signals generation," *Opt. Exp.*, vol. 30, no. 15, pp. 27132–27139, Jul. 2022.

[20] C. Ma, C. Tian, S. Li, Z. Xie, X. Zhao, and Z. Zheng, "Tunable microwave pulse generation based on active mode-locked optoelectronic oscillator," *Opt. Exp.*, vol. 32, no. 20, pp. 35150–35158, Sep. 2024.

[21] Y. Zhang et al., "An active time-domain mode-locked optoelectronic oscillator based on intracavity polarization control," *J. Lightw. Technol.*, vol. 43, no. 7, pp. 3163–3170, Apr. 2025.

[22] Z. Zeng et al., "Controllable microwave pulse generation in actively mode-locked optoelectronic oscillator based on electro-optic dual-drive Mach-Zehnder modulator," *Opt. Exp.*, vol. 33, no. 4, pp. 8761–8773, Feb. 2025.

[23] Z. Zeng et al., "Multi-format microwave signal generation based on an optoelectronic oscillator," *Opt. Exp.*, vol. 29, no. 19, pp. 30834–30843, Sep. 2021.

[24] Z. Zeng et al., "Position-definable coherent microwave pulse train generation in an actively mode-locked optoelectronic oscillator," *Opt. Lett.*, vol. 50, no. 3, pp. 718–721, Jan. 2025.

[25] X. Li et al., "Broadband pulse generator based on a self-injection-locked Fourier domain mode-locked optoelectronic oscillator," *Opt. Commun.*, vol. 519, Sep. 2022, Art. no. 128433.

[26] D. Tang and L. Zhao, "Generation of 47-fs pulses directly from an erbium-doped fiber laser," *Opt. Lett.*, vol. 32, no. 1, pp. 41–43, Dec. 2007.

[27] F. Krausz, L. Turi, C. Kuti, and A. Schmidt, "Active mode locking of lasers by piezoelectrically induced diffraction modulation," *Appl. Phys. Lett.*, vol. 56, no. 15, pp. 1415–1417, Apr. 1990.

[28] P. Runge, C.-A. Bunge, K. Petermann, M. Schlak, W. Brinker, and B. Sartorius, "Widely tunable short-pulse generation with ultralong semiconductor optical amplifiers," *J. Lightw. Technol.*, vol. 28, no. 5, pp. 754–760, Mar. 2010.

[29] O. De Vries et al., "Acousto-optic pulse picking scheme with carrier-frequency-to-pulse-repetition-rate synchronization," *Opt. Exp.*, vol. 23, no. 15, pp. 19586–19595, Jul. 2015.

[30] J. Xie, Y. Lin, L. Yan, and B. Chen, "Femtosecond laser pulse picking method based on Mach–Zehnder modulator by keeping phase of the picked-up pulse steady," *IEEE Trans. Instrum. Meas.*, vol. 72, 2023, Art. no. 7008009.

[31] B. N. Nyushkov, S. M. Kobtsev, A. V. Ivanenko, and S. V. Smirnov, "Programmable optical waveform generation in a mode-locked gain-modulated SOA-fiber laser," *JOSA B*, vol. 36, no. 11, pp. 3133–3138, Oct. 2019.

[32] W. Lyu et al., "Pulse generation with programmable positions based on a phase-modulated optical frequency-shifting loop," *Opt. Lett.*, vol. 48, no. 13, pp. 3411–3414, Jun. 2023.

[33] S. Liu et al., "Optical pulse generation with programmable positions in an actively mode-locked optical cavity," *Opt. Lett.*, vol. 49, no. 22, pp. 6393–6396, Nov. 2024.

[34] X. S. Yao, L. Davis, and L. Maleki, "Coupled optoelectronic oscillators for generating both RF signal and optical pulses," *J. Lightw. Technol.*, vol. 18, no. 1, pp. 73–78, Jan. 2000.

[35] X. S. Yao and L. Maleki, "Optoelectronic microwave oscillator," *J. Opt. Soc. Amer. B*, vol. 13, no. 8, pp. 1725–1735, Aug. 1996.